Atomic force microscope nanolithography: dip-pen, nanoshaving, nanografting, tapping mode, electrochemical and thermal nanolithography

2009 J. Phys.: Condens. Matter 21 483001

(http://iopscience.iop.org/0953-8984/21/48/483001)

J. Phys.: Condens. Matter **21** (2009) 483001 (18pp) doi:10.1088/0953-8984/21/48/483001

TOPICAL REVIEW

Atomic force microscope nanolithography: dip-pen, nanoshaving, nanografting, tapping mode, electrochemical and thermal nanolithography

Luis G Rosa[1,2,4] **and Jian Liang**[3]

[1] Department of Physics and Electronics, University of Puerto Rico-Humacao, 100 Road 908 CUH Station, Humacao, PR 00791, USA
[2] The Institute for Functional Nanomaterials, University of Puerto Rico, Facundo Bueso Building, Rio Piedras, PR 00931, USA
[3] Department of Biological Sciences, Columbia University, New York, NY 10027, USA

E-mail: luis.rosa13@upr.edu

Received 7 September 2009, in final form 12 October 2009
Published 6 November 2009
Online at stacks.iop.org/JPhysCM/21/483001

Abstract
Atomic force microscopy (AFM) has been widely employed as a nanoscopic lithography technique. In this review, we summarize the current state of research in this field. We introduce the various forms of the technique, such as nanoshaving, nanografting and dip-pen nanolithography, which we classify according to the different interactions between the AFM probe and the substrate during the nanolithography fabrication process. Mechanical force, applied by the tip to the substrate, is the variable that can be controlled with good precision in AFM and it has been utilized in patterning self-assembled monolayers. In such applications, the AFM tip can break some relatively weak chemical bonds inside the monolayer. In general, the state of the art for AFM nanolithography demonstrates the power, resolution and versatility of the technique.

(Some figures in this article are in colour only in the electronic version)

Contents

[4] Author to whom any correspondence should be addressed.

1. Introduction

The 'current state of the art'

In this review, we outline recent developments and some of the specific applications of atomic force microscope

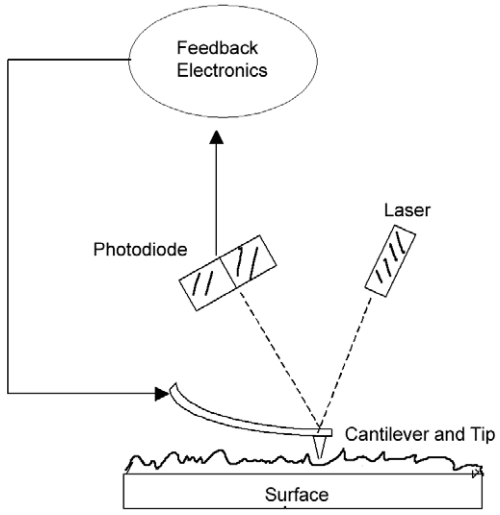

Figure 1. Schematic illustration of the atomic force microscope setup.

nanolithography. These techniques include nanoshaving, dip-pen, nanografting, tapping mode AFM nanolithography, electrochemical AFM nanolithography and thermal AFM nanolithography. Our emphasis is on nanolithography and deposition that involves organic materials and substrates as manifest in the wide variation of atomic force microscope nanolithography.

While atomic force microscopy (AFM) has attracted tremendous interest as an imaging tool since its invention in 1986 [1], AFM has other applications at the nanoscale [2]. The basic principles of AFM are relatively straightforward: an AFM uses a sharp tip, with a typical radius of curvature of its apex in the range of nanometers, mounted on a microscale cantilever, to scan the specimen surface (figure 1). When the tip is brought into the proximity of the sample surface, the forces between the tip and the sample lead to deflection (when the AFM is operated in static/contact mode), or modification of the vibrational motion (when the AFM is operated in dynamic or tapping/non-contact mode), of the cantilever.

In contact mode, the force can be calculated from the spring constant and the displacement of the cantilever on the basis of Hooke's law. Displacement of the cantilever is typically measured by the deflection of a laser beam from the back of the cantilever into a position-sensitive photodiode detector. The signal is then used, through a feedback loop, to control a piezoelectric stage that extends or retracts along the axial direction, maintaining the force at a constant set point value. In tapping mode, the cantilever is driven near its resonant frequency. The amplitude, frequency and phase of the oscillation shift because of the interaction between the tip and the surface, and this in turn provides an indication of the forces involved. Depending on the type of interaction between the tip and the surface, AFM is able to image and obtain a number of physical properties of the materials such as topography, friction, charge distribution, work function, local magnetic field, electronic spins and thermal conductivity. Many variations of AFM have been now developed including lateral force microscopy (LFM) [3], electrostatic force microscopy (EFM) [4], Kelvin probe force microscopy (KPFM) [5], magnetic force microscopy (MFM) [6], magnetic resonance force microscopy (MRFM) and scanning thermal microscopy (SThM) [7].

AFM has now advanced beyond use as an imaging tool to the direct manipulation of material, particularly at the nanometer scale. There have been many successful attempts to use AFM as a lithographic tool, thus providing one route for ultrahigh-resolution fabrication at selected surfaces. AFM nanolithography has proved so popular since the first papers on nanoshaving and dip-pen nanolithography were published, notably the paper in 1997 entitled 'Nanometer-scale fabrication by simultaneously nanoshaving and molecular self-assembly' by Xu [8] and the 1999 paper entitled 'Dip-pen nanolithography' by Piner [9], that it has led to over 850 papers in ten years. During this time, AFM nanolithography has been developed for the fabrication of nanostructures with features ranging from a few nanometers to hundreds of nanometers, and deposition of a large variety of substances like small organic molecules, polymers, nanoparticles, large biomolecules and inorganics on either metal or insulating substrate surfaces [10–14]. Atomic force microscope nanolithography could also be used as a direct writing technique where an AFM tip is used to deliver a substance directly to a nanosize region of a substrate. Because of its capabilities for nanofabrication [15–23], AFM nanolithography can be performed in diverse ambient conditions which have improved applications in molecular electronics, biomolecular arrays, biosensors and soft organic structure where the presence of ambient water plays a role in material transfer and preservation of biomolecules like DNA and proteins [24–27]. Besides ambient conditions, the environment for performing AFM nanolithography in can be modified by immersing the tip–substrate system in liquids such as organic solvents, water or buffers. AFM nanolithography has been successfully applied for various research purposes, for example: to make two-dimensional patterns within inorganic [28], organic [29, 30], or biological materials [31, 32]; to detect DNA hybridization at the nanoscale [33–35]; to confine de novo proteins onto gold surfaces [36, 37]; to build three-dimensional surface-bound biological assemblies; and to explore nanoscopic elasticity [38], friction [39], and the mechanical response to force modulation of organic thin films. It has also been used to characterize the shape of AFM tips and to measure the accelerated kinetics of thiols under nanografting conditions.

Atomic force microscope nanolithography is rather a simple nanofabrication technique, but the basic physical mechanisms for the process are still a matter of some debate. The main reasons for such complications are all related to the physical and chemical properties of the substances used for nanofabrication, the surface composition, water meniscus formation, the tip material and shape, the contact area, heat transfer through tip friction, the temperature, scanning speeds and the tip–surface applied force. The tip–surface meniscus formed will be affected either by a hydrophobic–hydrophilic substrate or by environmental relative humidity; therefore changing the meniscus size and shape changes the rate of transfer of material to the substrate. A general picture

of the material transfer from the tip to the surface is also debated and not completely established. It is understood from various studies that the formation of a liquid meniscus bridge promotes the material transfer from the tip to the surface, especially for dip-pen nanolithography [40–43], while for other methods in AFM nanolithography such as nanografting, which is performed immersed in liquids, it is clear that the mechanism of material transfer to the nanostructure sized region is dominated by diffusion.

2. A general overview of substrates and SAMs commonly used for atomic force microscope nanolithography

2.1. Organic silane complexes self-assembled on silicon oxide

In recent years the advances in self-assembled monolayer characterization and uses of these highly ordered films have extended from self-assembly on Au(111) to self-assembled layers on silicon oxide [44–50]. It is of relevance to mention that self-assembled layers on silicon oxide are currently playing a significant role in the fabrication of nanopatterned structures on these particular surfaces. An organic silane compound typical composition consists of a silicon atom tetrahedral bond, in which three of the bonds are to organic functional groups (alkoxy or ethyl groups). The fourth bond of the tetrahedral structure will be binding a functional group of some particular interest: anthracene, pentacene or pyridines for example [51, 52].

As a common procedure, polished surfaces of doped Si(100) wafers are pre-cleaned to remove organic contamination and particles. The wafers are immersed in Piranha solution (H_2SO_4:H_2O_2—1:1 by volume) to hydroxylate the silicon wafer surfaces, making them extremely hydrophilic. The native oxide surface is untouched by this procedure. The hydrophilic wafers are immersed in a solution of the organosilane compound. Cleaning procedures could vary among systems but excess molecules are generally removed by rinsing and sonicating in a fresh solvent, annealed at ∼50 °C in high humidity environments and immersed once more in the same silane solution, rinsed and sonicated and then finally baked at high temperature over 100 °C. The latter step aims to convert the hydrogen bonds of the adsorbed organosilane on a silicon oxide surface to covalent bonds. In the interaction of the silane and the SiO_2 surface, in contrast to the most common self-assembly of the thiol–Au bond here, the silane molecules condense with native hydroxyl groups on the SiO_2 surface, forming a thin layer of covalently linked polysiloxane at the interface. This bond on the SiO_2 is more stable physically than the thiol–Au bond.

2.2. Thiols on metal surfaces

Research into self-assembled monolayers of thiols [53] has in the last 20 years produced well over 130 papers a year. A wide variety of scientific studies have been carried out, ranging over molecular surface structure, electronic structure, dynamics of formation, nanofabrication and microfabrication, synthesis and chemical functionalization [54–57]. A number of thiols, both aromatic and aliphatic ones, have been self-assembled in different nanojunctions, especially because of their potential applications in molecular electronics [58, 59]. SAM layers are organic thin films grown on different substrates using molecules with a head group (typically an SH group) that has high vertical affinity to the surface (typically gold) but high lateral mobility, allowing the lateral packing of the molecules to be stabilized by intermolecular van der Waals forces. The *n*-alkanethiols and other functionalized thiols formed by adsorption on gold surfaces are generally well-ordered and crystalline. Upon exposure of a gold substrate to a thiol solution or in the gas phase, a bond between gold and sulfur (∼44 kcal mol^{-1}) [60] is formed. Typically, the dynamics of this reaction will occur within seconds to minutes. The surface is usually exposed to the thiol solution for a couple of hours or 24 h, contributing a significant amount of order during the assembly process into a closely packed structure, in the case of *n*-alkanethiols primarily in an all-*trans* configuration with a $(\sqrt{3} \times \sqrt{3})$ surface structure and chain tilt angle with respect to the surface normal of ∼30°. At low surface coverage, the alkanethiolate molecules lie flat, with their hydrocarbon backbones parallel to the gold surface; at higher surface coverage, the molecules begin to stand up, with the hydrocarbon tails tilting approximately 30° from the surface normal and nominally in the all-*trans* configuration to maximize van der Waals interactions [61]. Self-assembled monolayers (SAMs) of *n*-alkanethiolates on silver surfaces, for example, are more tightly packed and have less of a tilt angle than those on Au(111). Thiol and dithiol SAMs are considered promising building blocks for constructing nanodevices because the SH groups at the top of the hydrocarbon chains offer the possibility of forming connections to other functional units, e.g. metal or metal oxide clusters [62–68], thin films [69–73] and other functional molecules [74, 75].

Typically, thiol self-assembled monolayers are prepared on a Au(111) surface generally prepared by thermal evaporation or sputtering on a mica substrate in vacuum at a background pressure of 1×10^{-7} mbar. Typically, 1000 Å of gold are deposited on freshly cleaved mica at the rates of 0.2–0.3 Å s^{-1}. During gold deposition, the vacuum will increase and then remain at 6–8 $\times 10^{-7}$ mbar. After metallization, the Au-coated mica is allowed to cool down to room temperature. Before the use of the gold substrate, if a flatter surface is needed, hydrogen flame annealing is commonly used before the substrate is exposed to the thiol solutions.

2.3. Langmuir film deposition

Langmuir–Blodgett films are currently used in efforts in parallel with AFM nanolithography [76–79]. Langmuir film preparation consists in the dispersion of organic or inorganic surfactants on an ultrapure water subphase. Surfactants are composed molecularly of a hydrophilic and a hydrophobic part, as on the water subphase the hydrophilic part is pulled into the bulk of the water and the hydrophobic part away from the water subphase, creating and determining an orientation along the surface normal of the water subphase. In order to increase

the surfactant ordering on the 2D water subphase, the surface tension of the system is increased by sweeping a barrier over the water surface, typically at a rate of 100 $cm^2\ min^{-1}$, and increasing the surface tension to tenths of millinewtons per meter. Large varieties of substrates are used, such as glass, metal and semiconducting substrates, graphite and silicon oxide.

2.4. The AFM nanolithography setup

The atomic force microscope main component is a microscale cantilever with a sharp tip, usually with an average tip diameter of 10–20 nm, used to scan the specimen surface; figure 1. The cantilever is typically silicon or silicon nitride. When the tip is brought into the proximity of a sample surface, forces between the tip and the sample lead to a deflection of the cantilever according to Hooke's law. Depending on the forces acting on the tip, the atomic force microscope is able to image and obtain physical properties such as topographical or surface structure information, friction, expansion and compression of the materials, magnetic and electrical properties and electrical transport. The sample image is typically generated by the deflection of a laser spot from the top surface of the cantilever into an array of photodiodes. The force acting on tip will cause the cantilever to deflect while the tip is being swept on the surface. The AFM can be operated in a number of modes, depending on the application. In general, possible imaging modes are divided into static (also called contact) modes and a variety of dynamic or non-contact (also called tapping) modes where the cantilever is vibrated. Nanostructuring and imaging are usually both carried out using the same AFM and tip.

2.4.1. Force calibration for AFM nanolithography. In contact mode AFM the tip scans in close contact with the surface; the forces on the tip are typically repulsive with mean values of nanonewtons. Also in contact mode AFM, the deflection of the cantilever is sensed and compared in a feedback amplifier to some desired value of deflection. If the measured deflection is different from the desired value, the feedback amplifier applies a voltage to the piezoelectric device (the 'piezo') to raise or lower the sample relative to the cantilever to restore the desired value of deflection. The voltage that the feedback amplifier applies to the piezo is a measure of the height of features on the sample surface. The loads are applied by applying a voltage to the piezo and consequently lowering the tip to the surface, causing an increase in the load force against the surface. The tip–surface force is generally dominated and described as a Hooke type force,

$$\langle F \rangle = k\,\Delta z, \tag{1}$$

were k is the cantilever spring constant, which is dependent on the tip geometry and composition [80–82], and Δz the change in displacement along the surface normal. To perform AFM nanolithography in contact mode, the normal load must exceed a certain threshold to allow the tip to penetrate the film and to induce the substitution reaction. Forces applied to nanostructures will start at tenths of nanonewtons and will vary depending on the material, surface composition and structure.

Tapping mode AFM requires a piezoelectric crystal in contact with the cantilever holder in order to drive through its resonant frequency oscillation on the tip. The piezo motion causes the cantilever to oscillate with amplitudes approximately larger than 20 nm in air away from the surface. The oscillating tip is then moved toward the surface until it begins to lightly tap the surface. During scanning, the vertical oscillating tip alternately contacts the surface and lifts off, generally at a frequency hundreds of kHz. As the oscillating tip begins to contact the surface, the cantilever oscillation is damped due to the lost of energy caused by the tip contacting the surface. The reduction in oscillation is then used to identify and measure surface features. In tapping mode AFM operation, the forces applied to the surface are controlled by the drive amplitude and the amplitude set point, for imaging and for AFM nanolithography. This force between the tip and the surface in the tapping mode is not necessarily well-defined since the tip–surface interaction is considered an average effect. The drive amplitude is defined as the amplitude of the voltage modulation applied to the piezo, which drives the cantilever vibration, and the amplitude set point is the rms (root mean square) voltage of the oscillating cantilever as measured from the output voltage on the photocell and maintained by a feedback loop. An estimate of the average force and oscillating amplitudes could be given as

$$\langle F \rangle = \frac{k}{2Q}\sqrt{A_0^2 - A^2} \tag{2}$$

where A is the amplitude set point, A_0 is the free oscillation amplitude of the cantilever which is proportional to the drive amplitude, where Q and k are the quality factor and force constant of the cantilever, respectively. The expression [131] leads to the conclusion that increasing the averaged tip–sample force will increase the drive amplitude or decrease the amplitude set point or both. This expression for the average force acting on the tip–surface interaction simply shows in a general relationship that the increasing or decreasing oscillating amplitude would increase or decrease the average force.

The k value is obtained from either experimental measurement or the manufacturer's specifications. The Q value is measured by tuning the cantilever and dividing the resonant peak frequency by the FWHM of the peak. Experimental values of A_0 and A are obtained from the calibration force plots of the piezo extension along the surface normal versus amplitude deflection (figure 2). Equation (2) can qualitatively clarify the amplitude modulation procedure during nanografting but cannot be used to accurately calculate the averaged tip–sample force because of the approximations used during the deduction of the equation [83, 84]. Because of the complexity of the theoretical analysis of the tip motion and the tip–surface interaction, the analytical description or numerical simulation of the force in tapping mode AFM is still a partially open question [85–88]. However, using equations (1) and (2) to estimate the normal load is still possible.

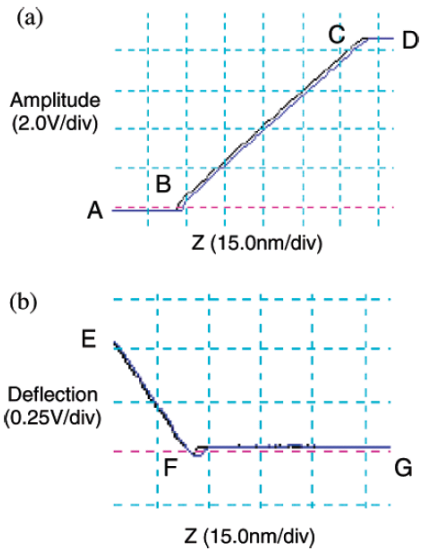

Figure 2. Plots of AFM tapping mode force measured in air. (a) Amplitude versus Z. (b) Deflection versus Z. The curves indicate the piezo extending and retracting directions, respectively.

3. Atomic force microscope nanolithography: different ways of 'writing'

3.1. Dip-pen nanolithography

Since the first paper in 1999 by Mirkin and his colleagues [9], dip-pen nanolithography (DPN) has been one of the most popular AFM nanolithography techniques, in which materials initially on the tip are transferred to the surface while scanning (figure 3) in either static or dynamic mode. DPN actually transplants the concept of writing with a pen to the nanoscale [89–92]. In this method, the AFM probe acts as a source of the 'ink'. DPN has been successfully applied with a variety of 'ink–substrate' combinations. Inks used for DPN range from small organic molecules to organic and biological polymers and colloidal particles, while substrates can be metals, semiconductors, insulators or other functional monolayers adsorbed on a variety of surfaces [13, 14, 9, 16, 18, 49, 92]. For ink materials with high melting points, a heated tip can be used to enhance the mobility of the molecules. The transferred molecules can just physically adsorb on the substrate or react with the surface species and form chemical bonds.

The mechanism of the tip–substrate molecular transport is still under debate and likely to be influenced by numerous parameters, including the composition of both the ink and the surface, the nature of the contact, the distribution and mobility of the ink on the tip, the water solubility of the ink, and the temperature and humidity at which the experiment is carried out. Besides these factors, the linewidths obtainable are also highly dependent on the writing speed. Although studies suggested that the material might diffuse through a water meniscus condensed between the tip and the substrate, writing experiments have also been performed at extremely low relative humidity or with molecules that are insoluble in water,

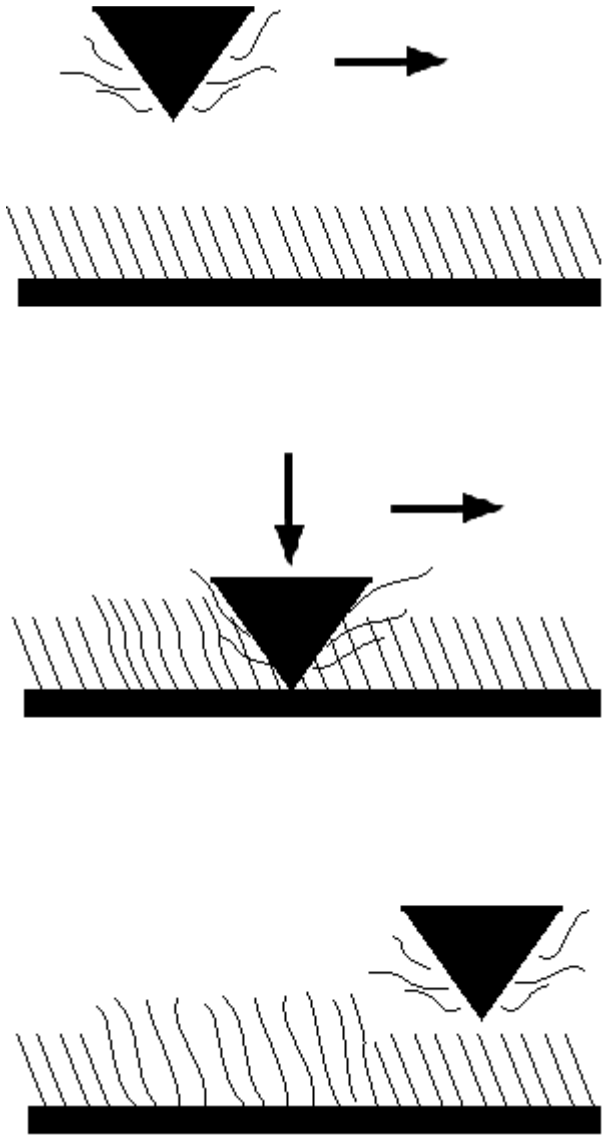

Figure 3. Schematic representation of dip-pen nanolithography, DPN.

which indicates the existence of other mechanisms [40–42]. Some theoretical models have also been put forward to simulate the condensation of a liquid meniscus between an AFM tip and a surface, and the diffusion of molecules at the nanometer sized contact. These studies would certainly provide more insights into the mechanism and thus enable reliable predictions of the dependence of DPN feature sizes on the various factors to be made. Interestingly, the water meniscus can be not just a transportation medium but also a reaction vessel. In some experiments, the target materials are synthesized *in situ* from precursors on the tip in the meniscus during the transfer process.

To improve the capacity and distribution of ink on the tip, some attempts have been made to integrate an ink storage and transfer system into the instrumentation. The prototype for such an experimental setup includes the attachment of a micropipette to the AFM cantilever. Later, with the help of other nanofabrication methods such as electron beam or

focused ion beam lithography, the integration of microfluid channels and reservoirs within the cantilever has been realized. Such micromachined fountain pens (MFP) have been used in DPN and for transfer of molecules into cells.

Like other scanning probe lithographic methods, DPN is a serial process, which has the drawback of slow speed in fabricating large-scale patterns. To increase the throughput and accessible area, parallel-probe cantilever arrays have been developed to realize multi-pen writing. The simplest implementation of parallel-pen DPN is a passive probe array. In this case, only one of the pens is actuated and all others passively follow the movement of the active one, duplicating a single pattern a number of times equal to the number of probes in the array. This design, however, requires extremely precise leveling of all the probes; otherwise some of the tips may contact at difference forces or just lose contact with the surface during scanning, resulting in heterogeneous linewidth, distortion and even missing of some of the drawings. Independent control of each probe tip is technically more complex, allowing complex patterns with better qualities, and may be accomplished using piezoelectric, capacitive, or thermoelectric actuation. Finally, yet importantly, the integration of microelectromechanical systems (MEMs) into DPN technology with the fountain-pen design can lead to the automation of tip coating and ink delivery. Since the mid-1990s, many multi-pen systems have been developed and the number of tips operated in parallel has grown dramatically. Parallel-dip-pen lithography with an eight-pen nanoplotter was reported by Mirkin and Hong in 2000 [93]. Recently, arrays of probes with as many as a million pens were produced. In another approach, ∼55 000 cantilevers were simultaneously aligned and used to pattern over square centimeter areas, and, as many as 450 000 000 sub-100 nm features were fabricated in less than 30 min. This massive increase in throughput will undoubtedly help with lowering the cost of large-scale fabrication by DPN and may lead to the final industrialization of the technique.

3.2. Electrochemical AFM nanolithography

An electrical bias between the AFM probe and the substrate can induce redox reactions on the surface species in the contact region (figure 4). Conductive tips made of a variety of materials, such as highly doped silicon, boron, diamond, tungsten, tungsten carbide, and gold- or platinum-coated silicon nitride, can be used in these experiments. Bias-assisted oxidation has been applied to a number of metals and semiconductors, in which the general reaction scheme can be summarized as follows:

$$\mathrm{M} + x\mathrm{H_2O} \rightarrow \mathrm{MO}_x + 2x\mathrm{H}^+ + 2x\mathrm{e}^- \quad (3)$$

$$2\mathrm{H_2O} \rightarrow \mathrm{O_2} + 4\mathrm{H}^+ + 4\mathrm{e}^- \quad (4)$$

$$2\mathrm{H_2O} + 2\mathrm{e}^- \rightarrow \mathrm{H_2} + 2\mathrm{OH}^- \quad (5)$$

where anodic reactions (equation (3)) and (equation (4)) occur at the substrate surface and the cathodic reaction (equation (5)) occurs at the tip. The water meniscus plays important roles in the reactions. Oxidation of organic resists, SAMs, and LB films is more delicate because it relies on various chemical functionalities of the molecules. For instance, terminal vinylic groups of an 18-nonadecenyltrichlorosilane (NTS) monolayer, or methyl groups of octadecyltrichlorosilane (OTS), on a silicon wafer can be locally oxidized to carboxylic acid groups by a conductive AFM tip with an applied bias voltage. The reaction can be confirmed by subsequently imaging the area with lateral force microscopy (LFM), or by coupling of the resulting carboxylic group with a second monolayer on top. Under LFM, although the oxidized region does not show any topographic contrast, an increase in frictional signal can be observed because of the changes in local surface polarity. Jang and collaborators demonstrated that solid state oxidative cross-linking could be initiated by a bias potential, leading to nanoscale patterns of conducting polymers, which is considered interesting because of its potential applications in organic electronics. In another approach, the electrical potential first induces chemical reactions in the functional coating on the tip, which in turn triggers a subsequent reaction on the surface and completes the lithography process.

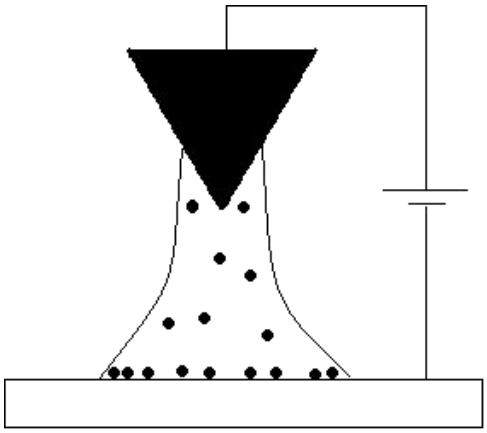

Figure 4. Schematic representation of electrochemical AFM nanolithography.

In most cases since 1999, dip-pens were used only to deliver organic molecular species to the surface. The ability to directly fabricate metal or semiconductor nanostructures on surfaces with a high degree of control over location and geometry is of significant interest in nanotechnology. Current industrial applications require the fabrication of devices with multiple metal and semiconductor components. Since there is a large interest in using atomic force microscope nanolithography techniques for writing of inorganic materials, Li and collaborators employed and introduced electrochemical dip-pen nanolithography [94]. The feasibility of using the new electrochemical dip-pen nanolithography directly for fabricating metal and semiconducting nanostructures on surfaces was demonstrated (figure 4). The technique as described by the authors is 'dip-pen' based and greatly improves the chemical diversity of the structures to be used as nanostructures on surfaces. Exploiting the use of the narrow gap between the tip and the surface and the formation of a meniscus due to capillary forces, Li and collaborators employed the water meniscus as a transfer medium for the

inorganic materials but also the tiny water meniscus was used as a nanometer sized electrochemical bath in which reduction of chemicals, electrochemically, by dissolving salts on the meniscus, is used to make nanometer-scale size patterns on surfaces.

In this pioneering approach to electrochemical AFM nanolithography by Li, the tip was dipped into a salt of H_2PtCl_6 and therefore dissolved on the water meniscus formed at the tip–surface interface. The salt was electrochemically reduced from Pt(IV) to metallic Pt ($PtCl_6^{2-} + 4e \rightarrow Pt + 6Cl^{-1}$), and the metal Pt was finally electrodeposited on a silicon oxide surface. The native oxide on the silicon wafer offers enough conductivity for the reduction. The nanostructure patterns fabricated through this method resulted in features of 30 nm on the plane of the surface, and along the surface normal the depositions were about ∼0.4 nm, demonstrating the high resolution and flexibility of the atomic force microscope nanolithography. Electrochemical dip-pen nanolithographies currently use various inks or salts for the electrodeposition of various metals such as Au, Ge, Ag, Cu, Pt, Pd, etc. As pointed out, in principle any metal or semiconductor that can be electrochemically deposited from a solution of salts could be deposited on a surface by electrochemical AFM nanolithography [95, 96].

Electrochemical AFM nanolithography can also induce the formation of chemical bonds between the ink and the substrate. For instance, Hurley *et al* [97] successfully used electrografting to covalently attach conjugated alkynes to silicon. The electrochemical cathodic reaction patterns the surface at the nanoscale with conductive-probe AFM, resulting in a monolayer with direct Si–C bonding is are very stable in air. Alkyne monolayer lines can be drawn down to 40 nm resolution using a Pt-coated tip, which opens up routes for delicate modifications of silicon surfaces with various organic molecules.

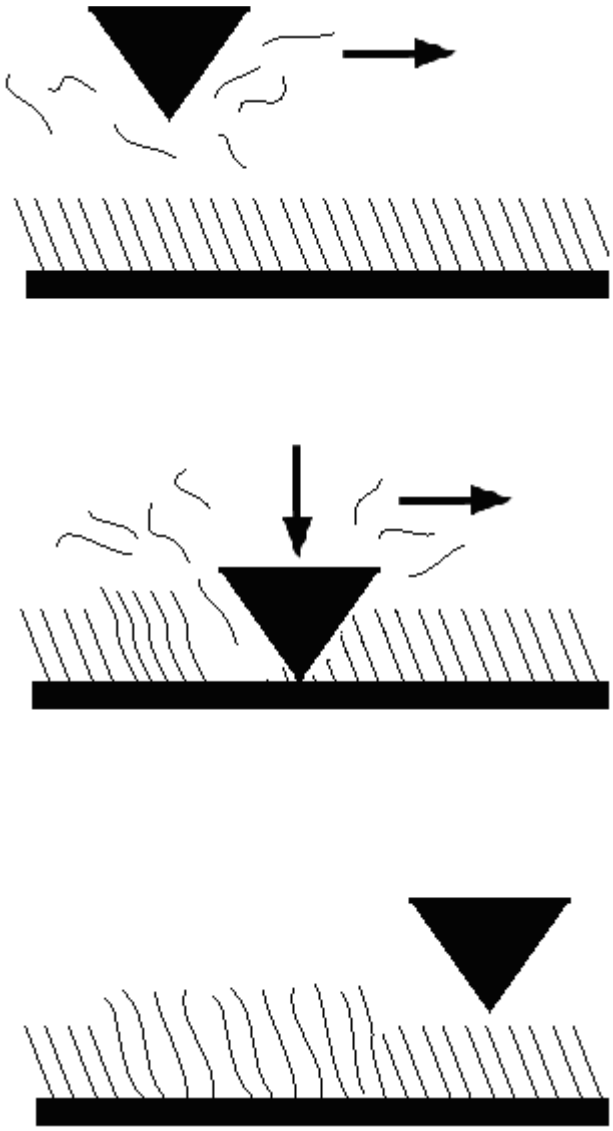

Figure 5. Schematic representation of nanografting.

3.3. Thermal AFM nanolithography

Thermal patterning requires a heated tip, which can be realized by focusing a laser beam onto it or integrating a resistor heater into the cantilever. When a heated tip that is in contact with a poly(methyl methacrylate) (PMMA) film reaches a temperature higher than the softening point, an indentation in the film is created that has the shape of the tip. The scientists at IBM have been developing the method for practical data storage. Patterning speed as well as read-out speed could be significantly increased by the development of multi-tip systems. In 2000, and again in 2003, Vettiger, Binnig and co-workers reported on the 'Millipede' system [98–101], which consists of an array of 1024 tips (32 × 32) with integrated read/write capabilities using combined effects of contact force and applied heat. The process of writing bits into thin PMMA films is achieved by heating the tips to 400 °C using a current traveling through a highly doped section at the end of the cantilever. This allowed the stressed lever structure to flex into the polymer. Read-out of the data was achieved by scanning a warm tip (300 °C) over the sample and measuring the heat resistance over the bits: when a tip entered a hole, the cantilever came closer to the PMMA film, thus increasing the heat conductivity. By combining 1024 tips on a 3 × 3 mm chip, patterns with a 12 mm pitch and 40 nm data bits corresponding to aerial densities of 400 Gb in^{-2} were obtained. The first prototypes of 4096-tip arrays (64 × 64; 6.4 mm^2) were already reported and design parameters are now focused on commercializing the concept. The presentation of the 'Millipede' system will probably be the first real commercial launch of an AFM-based 'nanostorage device', as long as issues of cost reduction and long-term operation can be resolved.

3.4. Nanografting: application on dithiol

Nanografting (figure 5) is an AFM nanolithography technique for fabrication of nanostructures on surfaces. Nanografting can be described as occurring in two important steps. The first step involves nanoshaving, in which the displacement of nanometer-scale selected portions of a thin film is achieved

(most commonly using SAM layers of thiols on Au(111)) by application of a carefully selected force. The desorbed molecules are discarded from the tip–surface contact region, as the solubility of the solute in a solvent such as ethanol or butanol is sufficiently high. The nanoshaving is followed by a second step in which fast self-assembly or deposition from solution onto the newly available open nanostructure surface site is carried out, leading to the reconstruction of a new monolayer. Experimental nanografting techniques have advanced significantly in the past few years, and as a result, applications of nanografting have been made to nanoelectronic devices [102], protein patterning, and biosensors [26, 27].

In the last ten years, a stream of publications have reported the structure and spectroscopic properties of dithiol SAMs [103–111]. The structure and spectroscopic properties of some thiols on surfaces have been obtained; nonetheless this research area still partially open. An important question still not fully answered is that of whether an −SH group at each end of the alkane chains will bind one or both sulfur atoms to the Au(111) surface. Two configurations are proposed and experimentally measured [103, 53]: one where both sulfur atoms are binding on the gold surface (the laying flat configuration) and another where a sulfur atom binds to the surface (the standing-up configuration). For most of the reported results two of the most common preparation methods in which self-assembly takes place were used: vacuum deposition and in liquid self-assembly [53, 103]. Another important question is that of whether the molecules would 'polymerize' during self-assembly. The basic polymerization proposed consists in forming a multilayer structure through intermolecular S–S bonds. Previous studies show for hexanedithiol no ordering in the standing-up configuration on Au(111) as measured using He diffraction, with disorder possibly caused by intermolecular S–S bonding [103]. Wöll *et al* [112] pointed out that direct self-assembly of dithiols on gold surfaces would result in disordered layers. They also suggested preparing the SAM by using dithiols with one of the SH groups being protected, and then removing the protecting groups after the formation of the SAM. Since a detailed investigation of the molecular orientation and adsorption kinetics of dithiols could shed considerable light on this subject, it could be very useful to visualize the dithiol thin films at the nanometer scale throughout their preparation process.

In order to shed light on the standing-up and lying flat configurations of the dithiol on Au(111) surfaces, Liang and collaborators [131] decided to try to solve this problem by using nanografting, which in combination with the AFM capabilities as regards topographic measurements provides an easily available reference of height. There is evidence in the literature [40] that nanografting can accelerate the kinetics of SAM growth and prepare SAMs with fewer defects than those prepared by self-assembly. Moreover, numerous experiments confirm that molecules in SAMs fabricated by nanografting assume well-predictable conformations. The authors apply nanografting to fabricate patches of dithiol layers in an inert matrix, establishing that nanografting is a very good method for making densely packed dithiol monolayers with good height homogeneity.

3.4.1. Self-assembly of decanedithiol (DDT) and biphenyldithiol (BPDT) from solution on gold surfaces. *In situ* self-assembly of DDT from a 0.1 mM 2-butanol solution onto an Au(111) surface is shown figure 6. During the self-assembly, *in situ* imaging is performed with the AFM tip which is retained with a controller normal applied force below 1 nN. The Au(111) surface is kept under fresh 2-butanol and then exposed by injecting a dithiol solution. As soon as the surface is exposed to the dithiol, which has nuggets with atomically flat tops, islands ranging from 10 to 50 nm in lateral dimension begin to appear. As the DDT (figure 7) self-assembles on the surface, the height of these islands steadily increases. Over time, it is observed that gradually the height exceeds half of the length of the dithiol, meaning that one of the sulfur atoms must be freed from the gold surface (figure 6(b)). The molecular chains can bend and tangle, which results in a poor degree of orientation [93], allowing enough degrees of freedom and possibly promoting disorder in the film.

As summarized in figures 6(c) and (d) the coverage increases over time through both nucleation and growth of previously formed nuclei. Images taken after 40 min of exposure, as shown in figure 6(c), illustrate that the dithiol islands grow up to lengths along the surface normal greater than the full length of a single molecule (1.76 nm; see figure 7) [113, 114]. In contrast to the self-assembling of alkanethiols, this growth over the molecular length can be explained by the linking of two molecules through the S–S bond. After 24 h, they can cover up to 10% of the area of the surface (figure 6(d)) and cannot be removed or reduced in size by being rinsed with pure ethanol or 2-butanol. The results suggest that thin films prepared in dithiol solution cross-link with each other due to the active −SH groups on each end. The S–S bonding of dithiol is the main cause of nucleation on top of the first layer formed. Following the same protocol, BPDT solution was exposed to the gold surface and the results are shown in figure 8. Similarly to the DDT case, the BPDT molecules also form islands that are much taller than a monolayer, indicating that BPDT can also polymerize through S–S coupling. The rate of formation of the islands is even quicker than that of DDT and after several hours, the initially separated islands begin to merge into bigger ones and cover the whole surface.

Liang and collaborators suggest that S–S bonding occurs in an oxidative coupling reaction of the form of $2R\text{–}SH + [O] \rightarrow R\text{–}S\text{–}S\text{–}R + H_2O$. Various methods has been suggested to prevent the oxidative coupling; Wang *et al* [115] tried to prevent the S–S coupling of dithiols by preparing the SAMs under an inert gas atmosphere. However, typical N_2 filled glove boxes have traces of O_2 in concentrations of approximately 100 ppm. The amount is small from a macroscopic view, but not negligible for a two-dimensional SAM. These results suggest that self-assembly of dithiol under inert gas protection is questionable, probably because: (1) there are always trace amounts of impurities which are sufficient to initiate the oxidative coupling due to the extremely limited number of molecules in a monolayer; (2) although the whole preparation process is carried out in N_2, the sample is exposed to air in the later imaging by AFM (which is also commonly the

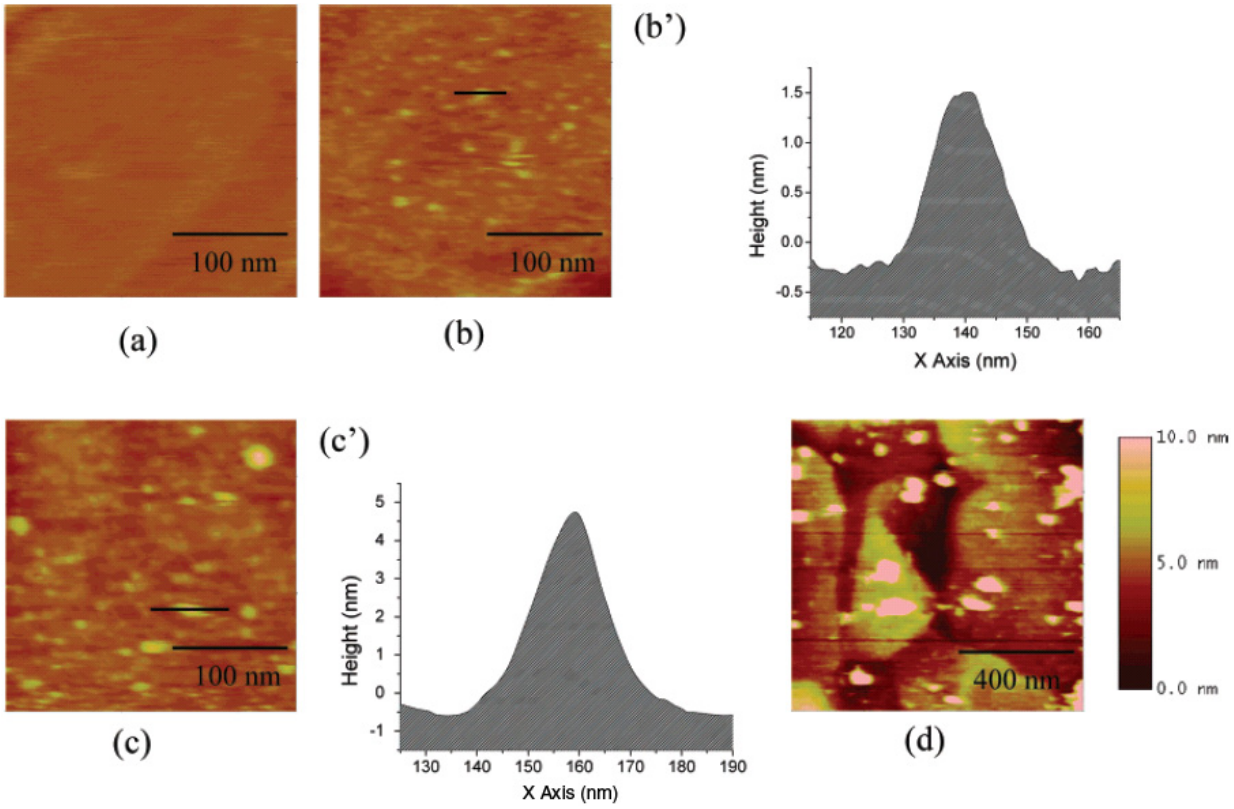

Figure 6. *In situ* imaging during the process of formation of the DDT layer from solution onto a Au(111) surface. Because of the drift of the AFM, the images are not focused on exactly the same region. Parts (b′) and (c′) show the line profiles corresponding to (b) and (c), respectively. (a) $t = 0$, (b) $t = 26$ min, (c) $t = 40$ min and (d) $t = 24$ h 2 min.

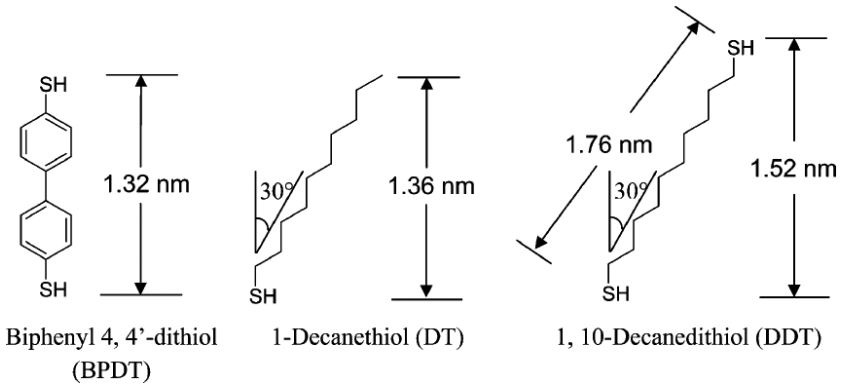

Figure 7. Structure and calculated dimensions of the molecules.

case in other applications or further treatment to the sample). Unfortunately, for both DDT and BPDT the nucleation on the gold surface is incomplete and randomly distributed rather than ordered and compact, and requires us to develop another way of fabricating fine-quality dithiol layers on gold surfaces.

3.4.2. Nanografting in solution of BPDT and DDT patches into a decanethiol (DT) SAM. The accelerated kinetics provided by nanografting influences the SAM formation through the space-confinement effect, and local pressures or temperatures developed during the process that are high enough to 'anneal' the molecules to form a compact layer. An advantage of the accelerated kinetics of SAM formation by nanografting is that it can make compact layers of thiols on the gold surface in minutes instead of days. Additionally, nanografting a molecule into a SAM matrix with a well-defined orientation (figure 7) along the surface normal provides a height reference for the new ones in the grafted patch. As a result the structure along the surface normal of the new molecule could be measured. The vertical height of the dithiol can be calculated from the difference between the patch and the matrix. The nanografted patches of BPDT on a DT matrix that resulted had significantly higher structure relative to that of the matrix (figures 9(a) and (a′)). Considering the atomic defects on the gold surface,

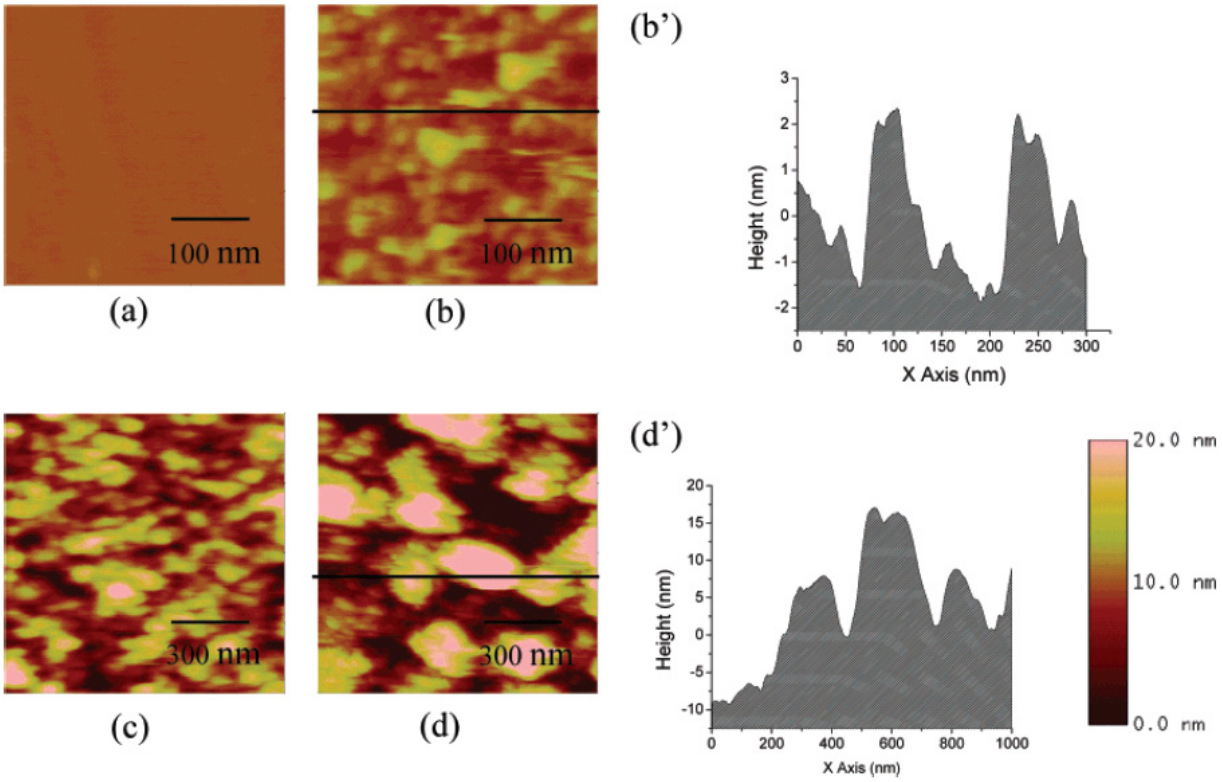

Figure 8. *In situ* imaging of the process of growth and formation of the BPDT layer from solution onto Au(111). Parts (b′) and (d′) show the line profiles corresponding to (b) and (d), respectively. (a) $t = 0$, (b) $t = 2$ min, (c) $t = 5$ h 0 min and (d) $t = 24$ h 1 min.

and the imperfection and the compressibility of the SAM, the error of the height measurement should be no more than 0.2–0.3 nm (the step height of Au(111) is 0.23 nm). As considered by the authors, deviations caused by the gold steps are small compared to those in the calculated model for the real nature of the SAM; the measured height difference is larger by an amount that is far beyond the error limits. A reasonable explanation, which is also supported by other spectroscopic studies [116, 117], is that the patch actually contains a multilayer instead of a monolayer of BPDT, as confirmed by a histogram of the height difference between the BPDT and DT, obtained by creating and making measurements on more than 200 patches (figure 9(c)). The envelope curve of the histogram can be fitted with two Gaussian peaks at 1.3 and 2.3 nm. The calculated thickness of a vertical bilayer and a trilayer of BPDT can be estimated at 2.3–2.6 nm and 3.4–3.9 nm, namely 0.9–1.3 nm and 2.0–2.5 nm higher than the DT monolayer, respectively, and completely consistent with the data. Although the structure of the multilayer is still poorly understood, a very large fraction of the BPDT patches had heights that were within the errors of those calculated for films containing two or three layers of BPDT.

In order to have a complete view of the multilayer formation nanografting of DDT on the DT matrix, also results from polymerization of the dithiol molecule are shown (figures 9(b) and (b′)). The histogram of figure 9(d) shows the lower probability of the formation of more than two layers for DDT. On the other hand, BPDT is more likely to form more than two layers. It is possible that the rigid structure and the π-stacking of the phenyl rings in BPDT help the molecule to form a more compact and ordered bottom layer. Consequently, the layer on top of it replicates the order and enhances the multilayer formation. On the other hand, the alkyl chains in the DDT layer are more flexible and less ordered because the bulky sulfur atoms prevent the chains from getting close to each other, which makes the forming of extra layers less favorable.

3.5. Nanoshaving

Mechanical scratching or nanoshaving may be the most straightforward way of performing nanolithography with AFM; in this process the tip is employed to displace materials from the sample surface, creating pits or trenches surrounded by walls consisting of the initial substrate material. It has been successfully applied to surfaces of metals, semiconductors and polymers. A necessary consideration in creating reproducible patterns is the durability of the tip itself, which is prone to deformation and contamination after repeated scanning. To avoid excessive wear, it has been proposed that tips composed of or coated with hard materials (e.g., diamond) or dynamic mode AFM should be used for such experiments.

3.5.1. The special case of selective nanoshaving on organosilane compounds self-assembled on SiO_2. Nanoshaving (figure 10) involves the displacement of nanometer-scale selected portions of a SAM by application of an AFM tip with a carefully selected force [37, 118–122]. The desorbed

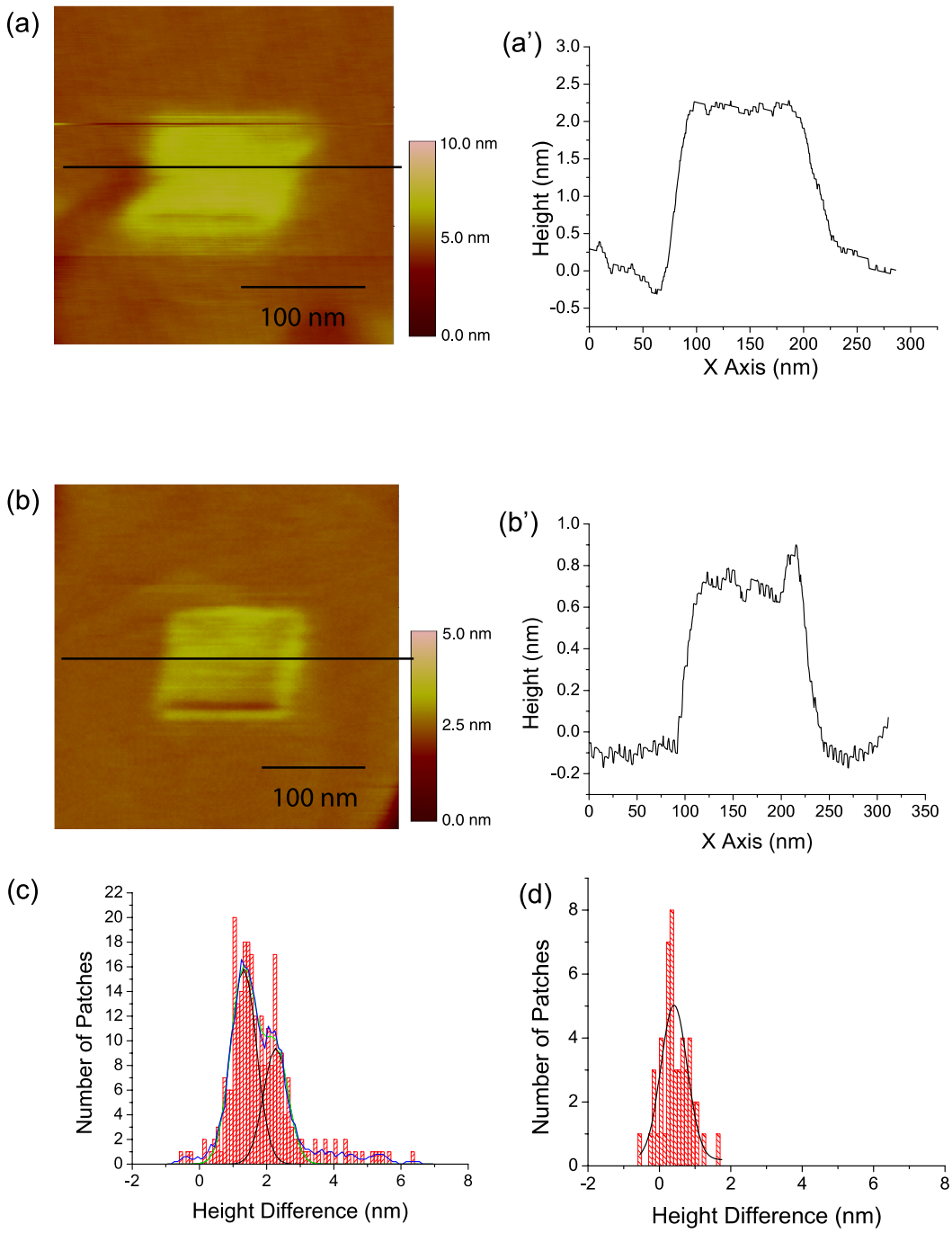

Figure 9. Images of the nanofabricated features of a 100 nm × 100 nm structure made by nanografting on the DT matrix and the corresponding line profiles. (a), (a′): BPDT, $\Delta h = 2.2 \pm 0.2$ nm. (b), (b′): DDT, $\Delta h = 0.8 \pm 0.2$ nm. Histogram (c) is constructed with height differences between BPDT and DT obtained from 232 BPDT patches. The envelope of the histogram, the two fitted Gaussian peaks, and the sum of the two fitted peaks are shown. Histogram (d) is constructed with height differences obtained from 49 DDT patches. The fitted Gaussian peak is shown in black.

molecules are discarded from the tip–surface contact region, as the solubility of the material in a solvent such as ethanol, butanol, water, etc is sufficiently high. While selective bond breaking of a variety of chemical species is known and has been demonstrated [8, 44, 123], the mechanical breaking of specific chemical bonds in an adsorbed species is more of a challenge [44]. Nanometer-scale lithography using an atomic force microscope (AFM) tip has been successfully demonstrated in the removal of material [69, 72, 73, 124, 125], often a self-assembled organic layer. While this type of nanoshaving leads to well-defined nanoscale features in a monolayer molecular film [126, 127], selective mechanical 'cutting' or bond breaking within the molecule, for only part of the molecular film, has not been demonstrated. Overcutting or etching using an AFM tip is certainly possible.

While thiolated molecules self-assembled onto Au(111) surfaces are very common, alkoxy silane species, with various end group ligands, have unique merits, as these

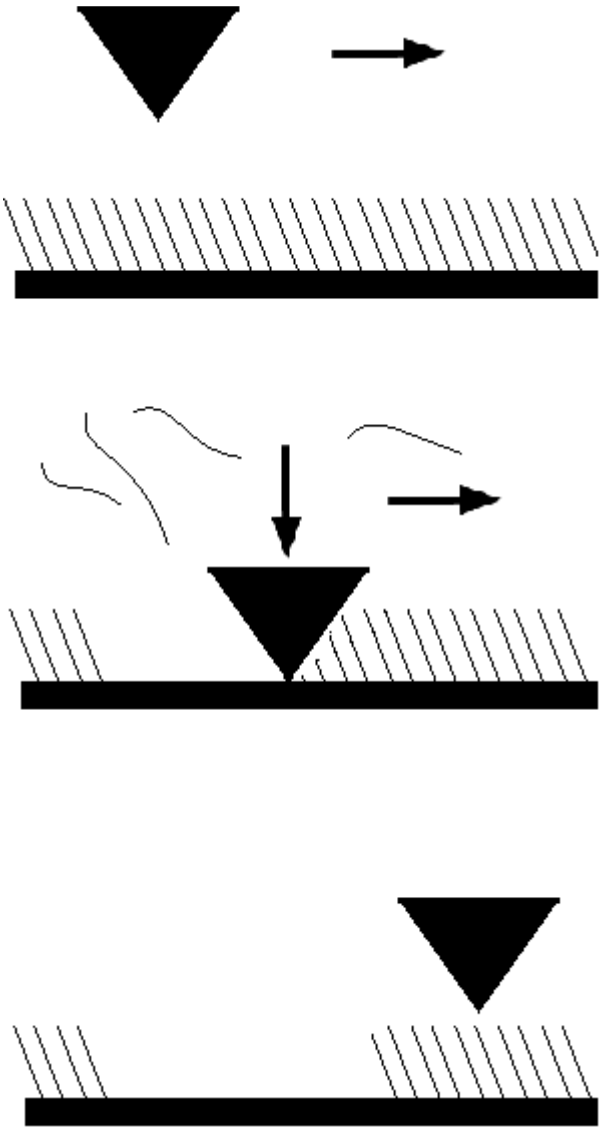

Figure 10. Schematic representation of nanoshaving.

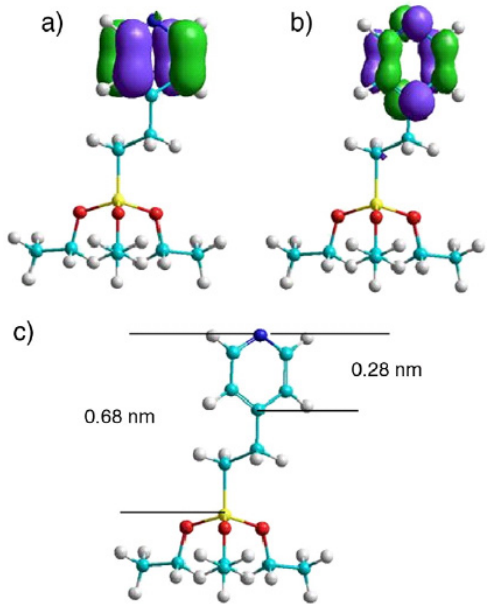

Figure 11. Structure of 2-(4-pyridylethyl)triethoxysilane. The HOMO–LUMO band gap is dominated by states originating from the pyridine terminal of the 2-(4-pyridylethyl)triethoxysilane molecule as indicated by the HOMO (a) and LUMO (b). The calculated structure and vertical distance along the surface normal for 2-(4-pyridylethyl)triethoxysilane adsorbed on silicon oxide (c). Worth noting are the width of pyridine at 0.28 nm and the vertical distance of 0.68 nm between the N of the pyridine and the Si.

molecular complexes form strong bonds with an oxide surface and can be used to modify both the dielectric properties and the optical properties of the surface [128]. 2-(4-pyridylethyl)triethoxysilane molecules, schematically shown in figure 11, were used to demonstrate a selective mechanical cutting of molecular layers on SiO_2. Using nanoshaving for selective mechanical bond breaking of an adsorbate has several requirements: the molecular unit composing the SAM layer should be well-anchored to the substrate and a rigid molecular backbone with at least one fairly 'weak' bond where the AFM tip can 'shear' off part of the molecule is needed. In addition, if the cleaved fragment is either volatile or 'sticky', then the shaved area can be prepared largely free of fragment debris. The complications that need to be avoided in the selective mechanical 'shearing' process are the removal or displacement of all of the adsorbate species (as opposed to shaving off a portion of the molecule), and the mechanical canting or 'tipping' of the orientation of the adsorbate species.

Combined photoemission (UPS) and inverse photoemission (IPES) (figure 12) spectra were taken for different coverages of 2-(4-pyridylethyl)triethoxysilane on the silicon oxide substrate, for coverage nominally up to one monolayer. The combined ultraviolet photoemission spectroscopy (UPS) and inverse photoemission spectroscopy (IPES) measurements provided an indication of the molecular orbital placement for both occupied and unoccupied orbitals for 2-(4-pyridylethyl)triethoxysilane, as indicated in figure 12. With repeated cycles of 2-(4-pyridylethyl)triethoxysilane exposure to the silicon oxide, the highest occupied molecular orbital (HOMO) to lowest unoccupied molecular orbital (LUMO) gap is seen to increase and features associated with the 2-(4-pyridylethyl)triethoxysilane molecular orbitals are evident and dominate the states measured in the UPS and IPES spectra. As demonstrated from the surface-sensitive electron spectroscopies, the pyridine electronic states are dominant as regards the band gap of the material and thus the AFM tip surface interaction during nanoshaving would be dominated by the pyridine group rather than the silane group of the molecule (figure 1).

The process of nanoshaving has been described extensively elsewhere [8, 44, 123]. As shown by Rosa for selective nanoshaving, an AFM tip was used with a SiN cantilever and a 0.58 N m^{-1} spring constant, so in the low force contact mode, the surface morphology could be imaged figure 13(a). To perform nanoshaving, load forces of 50 to 110 nN were applied by the tip to the SAM layer surface. In this force range, a complete scraping off of the 2-(4-pyridylethyl)triethoxysilane molecular film was not observed; rather nanoshaving cut depths of 0.64 nm were seen and to a lesser extent cut

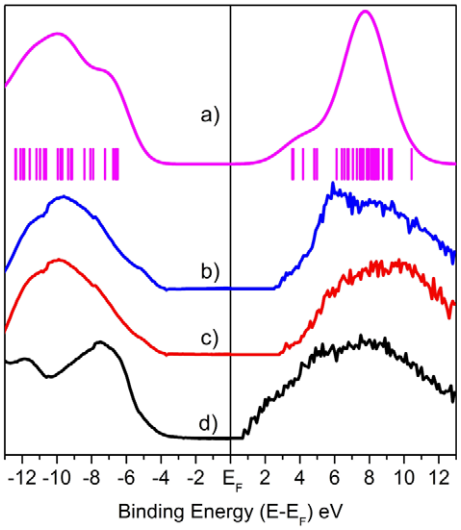

Figure 12. The electronic structure of 2-(4-pyridylethyl)triethoxysilane from combined photoemission and inverse photoemission spectroscopy, as a function of 2-(4-pyridylethyl)triethoxysilane coverage; the clean silicon oxide (SiO_2) substrate formed on p-doped silicon (a) can be compared to the surface half-coverage of 2-(4-pyridylethyl)triethoxysilane (b) and the full surface coverage of 2-(4-pyridylethyl)triethoxysilane (c). The experimental electronic structure (c) is also compared with the calculated density of states based on a single isolated molecule (d). The theoretical eigenvalues are shown below the expected density of states, uncorrected for solid state and matrix element effects.

depths of 0.27 nm. As illustrated in the AFM image in figure 13, a 100 nm × 100 nm nanoshaved region of 2-(4-pyridylethyl)triethoxysilane film can be imaged, showing sharp boundaries. The height profile or cross-section of the nanoshaved area or patch indicated (figure 13(b)) provides no indication of molecular canting induced mechanically.

Indeed, the compilation of AFM nanoshaving experimental results (figure 13(c)) for 2-(4-pyridylethyl)triethoxysilane thin films suggests that there is selective mechanical cleavage of the 2-(4-pyridylethyl)triethoxysilane molecular film at 0.64 ± 0.06 nm depth (figure 13(c)) or at the Si–C bond, as indicated in figure 11, with a minority of nanoshaving experiments leading to a cut depth of 0.28 ± 0.05 nm. At 50 nN applied force, the cut depths were observed to all be near the value of 0.28 nm. At 100 nN applied force, most of the nanoshaving cut depths observed were at 0.68 nm. The bond energies at the pyridine to ethyl 'neck' at a depth of 0.28 nm and at the siloxy–ethyl bond at an expected depth 0.68 nm are relatively weak at 71 and 76 Kcal mol^{-1} [129], so these are both likely mechanical cleavage points for a molecule oriented with the long molecular axis perpendicular to the shear direction (as is the case here). Since the molecular orbitals of the pyridine end group dominate the highest and lowest molecular orbitals, the pyridine end group should dominate the interaction with the AFM probe tip, thus aiding the mechanical nanoshaving process. What is clear is that it is now possible, with the correct choices of the anchor end group for the substrate, linking groups and the force applied to the AFM tip, that chemically selective nanoshaving can be achieved. At present, an accurate assessment of the shear

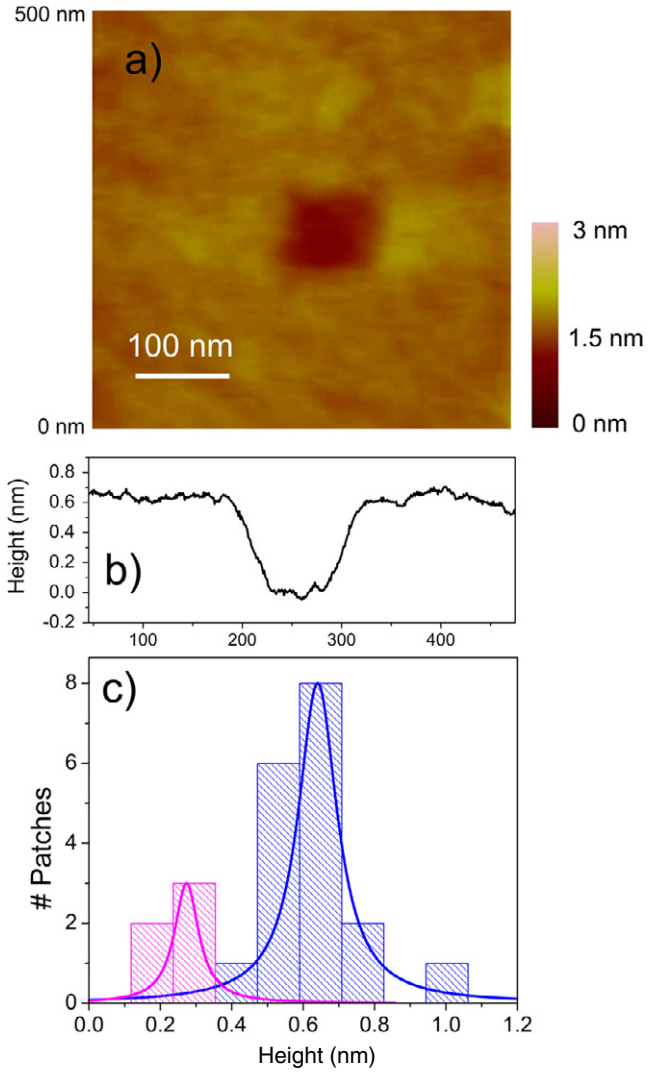

Figure 13. Nanoshaving of 2-(4-pyridylethyl)triethoxysilane monomolecular films. An AFM image of a 100 nm × 100 nm nanoshaved region of 2-(4-pyridylethyl)triethoxysilane is shown in (a), with the height profile or cross-section of the nanoshaved area or patch indicated in (b). A compilation of AFM nanoshaving experimental results for 2-(4-pyridylethyl) triethoxysilane thin films, as a histogram of the cut depth measurements taken from height profiles (c). The histogram was fitted with two Gaussians with peak centers at 0.28 and 0.64 nm, as indicated in panel (c).

forces is needed for this selective mechanical bond breaking and this remains a matter of some interest.

3.5.2. Tailoring the layer-by-layer structure of the dithiol multilayer by AFM tip nanoshaving in air and by adding antioxidant during nanografting in solution. Although nanografting cannot eliminate the oxidative coupling of dithiols, the patches of layers are uniform in height, which offers a better starting point for tailoring the layer-by-layer structure. In a recent approach, patches of biphenyl 4,4′-dithiol (BPDT) and 1,10-decanedithiol (DDT) are first dip-pen nanografted into a 1-decanethiol (DT) matrix under ambient conditions. In these molecular structures, one of the thiol groups forms Au–S bonds while the other is positioned on

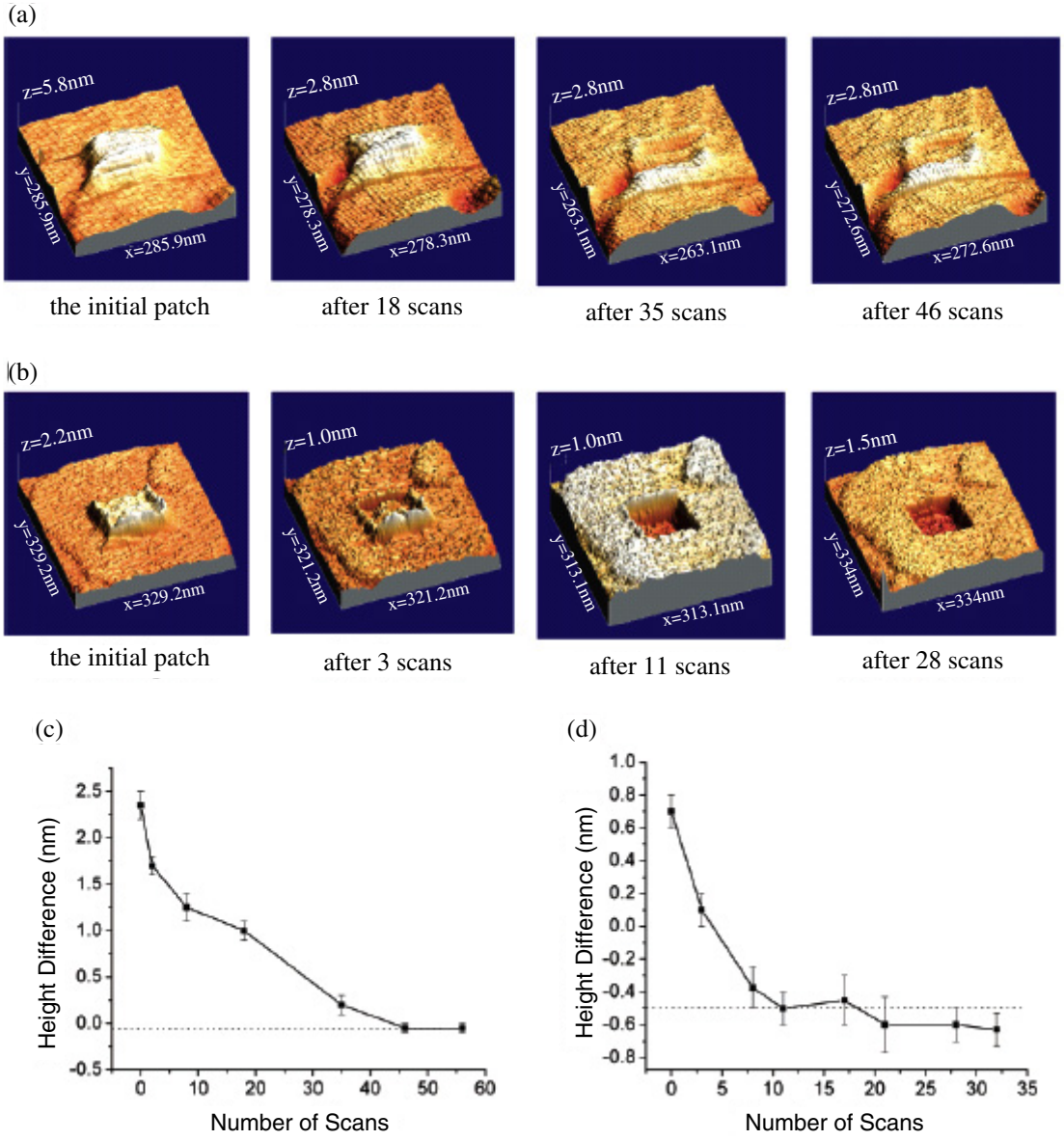

Figure 14. Three-dimensional images of nanoshaving sequences on (a) BPDT and (b) DDT multilayer patches within a DT matrix (normal force 8 nN).

top of the layer. The authors [123] attempted to shave away the extra layers in air with the AFM tip by applying a larger force load to the surface (but less than that in nanografting) and continuously scanned the region containing the patch after the dip-pen nanografting was performed. The typical patterns are, however, significantly higher than the thickness of a monolayer of BPDT or DDT. Due to oxidative coupling and formation of intermolecular disulfide bonds, a large fraction of the BPDT and DDT patches are composed of multilayers stacking on top of one another. Forces between 5 and 10 nN are not large enough for the tip to touch the gold but are large enough to deform the top layer and gradually remove molecules from it. The S–S linker, with a bond dissociation energy of 425 kJ mol^{-1}, is significantly weaker than the C–C bond (bond energy 618 kJ mol^{-1}) and susceptible to redox cleavage, being probably the most active point of the molecules in this situation. Figure 14 demonstrates how a BPDT patch and a DDT patch are lowered by continuous nanoshaving. The results indicate that the patches can be trimmed down to approximately monolayer height, but quantizing the number of layers is not at all simple, suggesting that the shaving of the top layer is not always complete. For both BPDT and DDT the height change slows down as the patch lowers, probably because the bottom layer is surrounded by the DT matrix and less accessible to the AFM tip. It is also worth noting that the height of the DDT patch decreases more quickly than that of the BPDT, implying that the BPDT molecules are packed in a more orderly fashion and harder to shave, as shown in figures 14(c) and (d).

3.6. Tapping mode AFM nanolithography of alkanethiols

Tapping mode atomic force microscopy operates by means of a vibrating cantilever near its resonant frequency (typically

100 kHz) touching the surface only at the bottom of each oscillating cycle, offering a less damaging imaging method. In today's advanced microscopy techniques, tapping mode AFM is commonly used as a method for imaging surfaces made of soft materials, including proteins, DNA, polymers and numerous other molecules and inorganic hard materials. Remarkably, the tapping mode AFM technique has also been successfully employed for manipulating nanoparticles, dissecting biomolecules, etching polymer thin layers and performing nanolithography, such as the nano-oxidation of silicon surfaces, and dip-pen nanopatterning.

The increasing interest in confining biomolecules to surfaces via AFM nanolithography such as nanografting for the purpose of biosensor fabrication or investigating electrical and mechanical properties has proved to be difficult, requiring an extraordinarily careful control of the normal load to avoid damaging the grafted biomolecules after a few scans. Biomolecules will denature upon change of the chemical environment or physical changes such as structure modification by temperature or applied pressure (forces). Particularly difficult (if possible) are experiments such as when the properties of a surface confined protein in a given patch are to be imaged many times in the same experimental run. Previously, few attempts to apply tapping mode AFM to nanografting have been reported [130, 131].

Liang *et al* [115] has demonstrated the applicability of tapping mode AFM to basic nanografting of 1-octadecanethiol (C18SH) into 1-decanethiol (C10SH) using tapping mode AFM in solution and dip-pen techniques. Alkyl thiols are excellent candidates for AFM nanolithography use. The authors demonstrated two important issues. First, tapping mode nanografting can be applied in the fabrication of thiol monolayers with well-predictable configurations. Second, tapping mode nanografting is possible by controlling the average normal force. To evaluate the quality of the acquired patterns, the heights of the patches are statistically analyzed and are compared with the calculated height difference of the two molecules. The control of the normal force, which is a key issue in nanografting, is not trivial because, in tapping mode, the cantilever oscillates at high frequency, which makes it more difficult to experimentally adjust and theoretically calculate the average interaction between the tip and the surface. The liquid medium also moves the vibrational frequency and amplitude of the cantilever resonance significantly to lower values from their values in air [132]. To avoid possible perturbations, the cantilever used for contact mode imaging should have the smallest force constant. This type of cantilever, however, has the lowest resonant vibration frequency when used in tapping mode and consequently is more likely to be affected by the environmental noise and the limited bandwidth of the feedback loop of the microscope. Another reason for using stiff cantilevers in tapping mode AFM is that when operating in air, the adhesion force between the tip and the surface resulting from the meniscus (the water column from humidity) would stick the cantilever to the surface if its force constant was too low and, consequently, the feedback loop would not be able to respond properly.

A long chain of alkanethiols has been proven to be produced by various experimental techniques, forming a stable

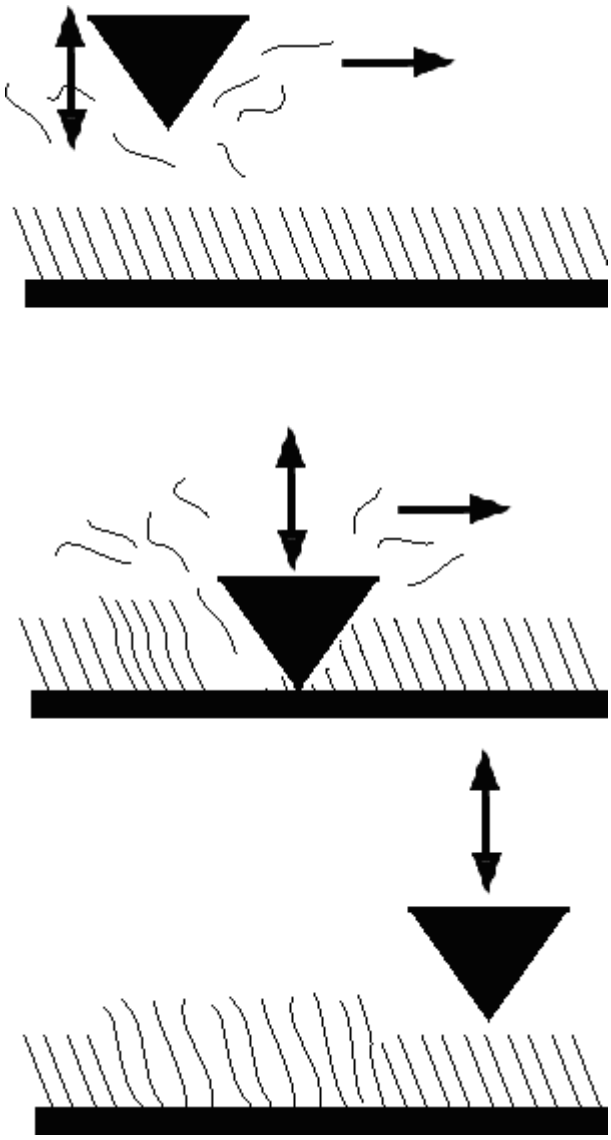

Figure 15. Schematic representation of tapping mode AFM nanolithography.

crystalline SAM layer and having a standard tilting angle of 30° with respect to the surface normal [95, 96]. In these experiments, $C_{18}SH$ alkane thiols were chosen to be used for tapping mode nanografting, as schematically shown in figure 15. It is common practice to measure the height difference between the nanopatterned regions and the matrix SAM, which was chosen to be C10SH alkane thiol; the height of the grafted molecules can be determined, and the conformation can be deduced. If the height difference agrees with the well-established model, this means that tapping mode nanografting, similarly to contact mode nanografting, can be used as an AFM fabrication technique. The height structural difference along the surface normal between $C_{18}SH$ and $C_{10}SH$ has been established, both by theory and by experiment, to be 0.9 nm [29]. Figure 16(a) show a typical image of a $C_{18}SH$ patch in a $C_{10}SH$ SAM made by nanografting using the tapping mode in solution. The cross-sectional analysis (figure 16(b)), which makes direct height measurements of topographic

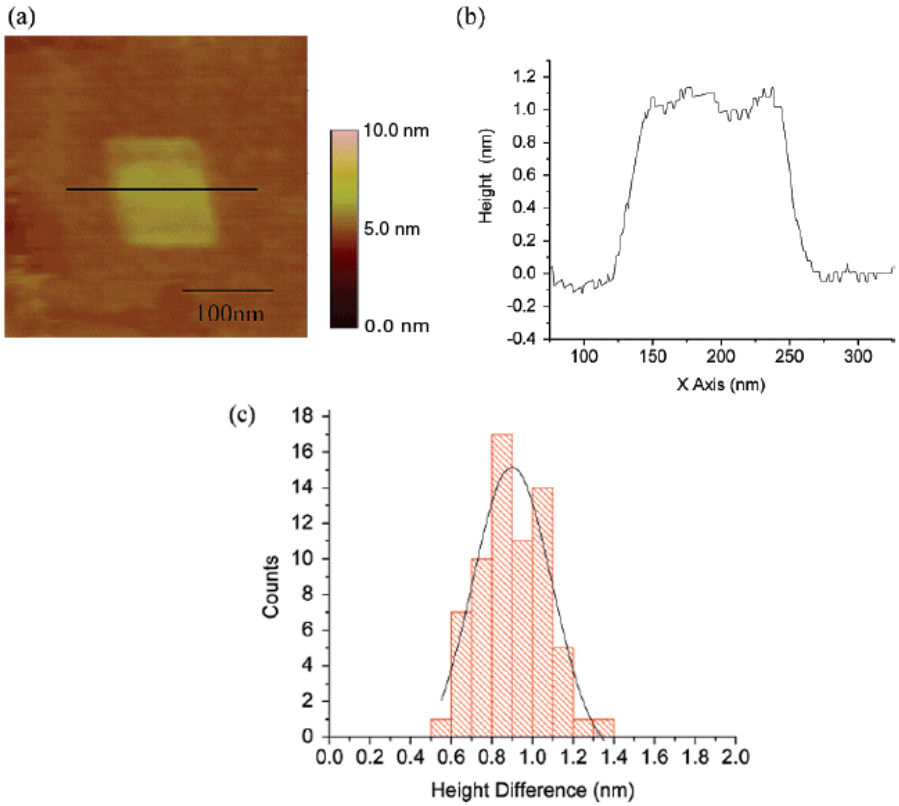

Figure 16. AFM tapping mode nanografting. (a) The height image of a typical $C_{18}SH$ patch (100 nm × 100 nm) in the $C_{10}SH$ matrix. (b) The corresponding line profile ($\Delta h = 1.0 \pm 0.2$ nm). (c) The histogram based on 67 patches, a fitted Gaussian curve and the peak position at 0.90 nm.

features by producing line profiles and averaging over them, indicates that the height difference between the $C_{18}SH$ and $C_{10}SH$ is 1.0 nm, in fair agreement with the calculated value. The Gaussian fit of the histogram (figure 16(c)) clearly shows a peak at 0.9 nm. The statistics also indicates that the average height difference is 0.9 nm with the standard deviation of 0.16 nm, which confirms that nanografting in the tapping mode can fabricate patches of layers with well-predictable molecular configurations.

Although AFM nanolithography in solution is common in most cases, in air it is also useful because it is experimentally simple. Ambient conditions are also low cost environments if the materials are stable and could be used for the fabrication of devices; currently most approaches operate in ambient conditions. Tapping mode nanografting in air can, therefore, be a good supplement to nanografting in solution. Nanografting in air requires the tip to be coated by the molecules to be used for nanofabrication [133]. When the applied force exceeds the threshold, the molecules will transfer and bind to the surface, replacing the initial molecules.

4. Conclusions

AFM nanolithography is an outstanding nanofabrication technique with a combination of resolution and versatility. It not only has been a powerful tool in the laboratory for scientific discovery, but also has great potential in industrial applications with the development of arrays of AFM probes that may realize massively parallel patterning. Exploration into the mechanism of the lithography process can help understand material transfer, mechanical deformation and chemical reactions at the nanoscale. As a top-down approach, lithography represents an important surface patterning technique, which was firstly introduced on the macroscale. In particular, the versatility of the technique results from the unrestricted interactions between the surface and the AFM probe. The probe plays various roles in the fabrication process, which, interestingly, share some common characteristics with some macroscale objects. Probably when a new analogy is drawn, a new route for the application of the technique will be opened.

Nanometer-scale lithographies, using an atomic force microscope (AFM) tip, have been successfully demonstrated in the removal of material [124, 125], often a self-assembled organic layer. This type of lithography leads to well-defined nanoscale features in a monolayer molecular film [126, 127], and achieves selective bond breaking at the molecule–substrate interface or within the molecule in the organic thin film. Overcutting or etching using an AFM tip is certainly possible, but mechanically engineering the organic surface selectively within the monomolecular layer opens up new vistas for nanoscale selective surface chemistry.

Acknowledgments

The National Science Foundation (MRSEC Program) through the Princeton Center for Complex Materials (DMR 0213706),

the DOE under Grant No. DE-FG02-93ER45503, the National Science Foundation (MRSEC Program) through the University of Nebraska-Lincoln (DMR 0820521) and the National Science Foundation Institute for Functional Nanomaterials in Puerto Rico (IFN; EPS 0701525) supported the authors' work.

References

[1] Binnig G, Quate C F and Gerber C 1986 *Phys. Rev. Lett.* **56** 930–3
[2] Samori P 2004 Scanning probe microscopies beyond imaging *J. Mater. Chem.* **14** 1353–66
[3] Carpick R W and Salmeron M 1997 *Chem. Rev.* **97** 1163
[4] Butt H J 1991 *Biophys. J.* **60** 777
[5] Nonnenmacher M, O'Boyle M P and Wickramasinghe H K 1991 *Appl. Phys. Lett.* **58** 2921
[6] Rugar D, Mamin H J, Guethner P, Lambert S E, Stern J E, McFadyen I and Yogi T 1990 *J. Appl. Phys.* **68** 1169
[7] Majumdar A 1999 *Annu. Rev. Mater. Sci.* **29** 505
[8] Xu S and Liu G 1997 *Langmuir* **13** 127–9
[9] Piner R D, Zhu J, Xu F, Hong S and Mirkin C A 1999 *Science* **283** 661–3
[10] Zhou D, Bruckbauer A, Ying L, Abell C and Klenerman D 2003 *Nano Lett.* **3** 1517–20
[11] Rezek B, Ukraintsev E, Michalíková L, Kromka A, Zemek J and Kalbacova M 2009 *Diamond Relat. Mater.* **18** 918–22
[12] Liu G-Y and Amro N A 2002 *Proc. Natl Acad. Sci.* **99** 5165–70
[13] Wilson D L, Martin R, Hong S, Cronin-Golomb M, Mirkin C A and Kaplan D L 2001 *Proc. Natl Acad. Sci.* **98** 13660–4
[14] Rosi N L and Mirkin C A 2005 *Chem. Rev.* **105** 1547–62
[15] Koumoto K, Saito N, Gao Y, Masuda Y and Zhu P 2008 *Bull. Chem. Soc. Japan* **81** 1337–76
[16] Ginger D S, Zhang H and Mirkin C A 2004 *Angew. Chem. Int. Edn* **43** 30–45
[17] Gates B D, Xu Q, Love J C, Wolfe D B and Whitesides G M 2004 *Annu. Rev. Mater. Res.* **34** 339–72
[18] Hong S and Mirkin C A 2000 *Science* **288** 1808–11
[19] Gu Z, Huang S and Chen Y 2009 *Angew. Chem. Int.* **48** 952–5
[20] Geissler M and Xia Y 2004 *Adv. Mater.* **16** 1249–69
[21] Hamley I W 2003 *Angew. Chem. Int.* **42** 1692–712
[22] Hon K K B, Li L and Hutchings I M 2008 *CIRP Ann.—Manuf. Technol.* **57** 601–20
[23] Krämer S, Fuierer R R and Gorman C B 2003 *Chem. Rev.* **103** 4367–418
[24] Wang Y, Mirkin C A and Park S J 2009 *ACS Nano* **3** 1049–56
[25] Leggett G J 2005 *Analyst* **130** 259–64
[26] Staii C, Wood D W and Scoles G 2008 *Nano Lett.* **8** 2503–9
[27] Staii C, Wood D W and Scoles G 2008 *J. Am. Chem. Soc.* **130** 640–6
[28] Garno J C, Yang Y, Amro N A, Cruchon-Dupeyrat S, Chen S and Liu G-Y 2003 *Nano Lett.* **3** 389
[29] Liu J-F, Cruchon-Dupeyrat S, Garno J C, Frommer J and Liu G-Y 2002 *Nano Lett.* **2** 937
[30] Wang X, Zhou D, Rayment T and Abell C 2003 *Chem. Commun.* **4** 474
[31] Garno J C, Amro N A, Wadu-Mesthrige K and Liu G-Y 2002 *Langmuir* **18** 8186
[32] Jang C-H, Stevens B D, Carlier P R, Calter M A and Ducker W A 2002 *J. Am. Chem. Soc.* **124** 12114
[33] Zhou D, Sinniah K, Abell C and Rayment T 2002 *Langmuir* **18** 8278
[34] Zhou D, Sinniah K, Abell C and Rayment T 2003 *Angew. Chem. Int. Edn* **42** 4934
[35] Liu M and Liu G-Y 2005 *Langmuir* **21** 1972
[36] Case M A, McLendon G L, Hu Y, Vanderlick T K and Scoles G 2003 *Nano Lett.* **3** 425
[37] Hu Y, Das A, Hecht M H and Scoles G 2005 *Langmuir* **21** 9103
[38] Jourdan J S, Cruchon-Dupeyrat S J, Huan Y, Kuo P K and Liu G-Y 1999 *Langmuir* **15** 6495
[39] Houston J E, Doelling C M, Vanderlick T K, Hu Y, Scoles G, Wenzl I and Lee T R 2005 *Langmuir* **21** 3926
[40] Ryu S and Schatz G C 2006 *J. Am. Chem. Soc.* **128** 11563–73
[41] Giam L R, Wang Y and Mirkin C A 2009 *J. Phys. Chem.* A **113** 3779–82
[42] Yu J-J, Tan Y H, Li X, Kuo P-K and Liu G-Y 2006 *J. Am. Chem. Soc.* **128** 11574
[43] Xu S, Laibinis P E and Liu G-Y 1998 *J. Am. Chem. Soc.* **120** 9356
[44] Rosa L G, Jiang J, Lima O V, Xiao J, Utreras E, Dowben P A and Tan L 2009 *Mater. Lett.* **63** 961–4
[45] Smith R K, Lewis P A and Weiss P S 2004 *Prog. Surf. Sci.* **75** 1–68
[46] Onclin S, Ravoo B J and Reinhoudt D N 2005 *Angew. Chem. Int. Edn* **44** 6282–304
[47] Lee M V *et al* 2007 *Chem. Mater.* **19** 5052–4
[48] Headrick J E, Armstrong M, Cratty J, Hammond S, Sheriff B A and Berrie C L 2005 *Langmuir* **21** 4117–22
[49] Lim J-H, Ginger D S, Lee K-B, Heo J, Nam J-M and Mirkin C A 2003 *Angew. Chem. Int. Edn* **42** 2309–12
[50] Luo M F, Su Y H, Hu G R, Nien C-H, Hsueh Y W and Chen P 2009 *Thin Solid Films* **517** 1765–9
[51] Jiang J Y, Lima O V, Pei Y, Zeng X C, Tan L and Forsythe E 2009 *J. Am. Chem. Soc.* **131** 900
[52] Ruckenstein E and Li Z F 2005 *Adv. Colloid Interface Sci.* **113** 43–63
[53] Laibinis P E, Whitesides G M, Allara D L, Tao Y T, Parikh A N and Nuzzo R G 1991 *J. Am. Chem. Soc.* **113** 7152–67
[54] Basnar B and Willner I 2009 *Small* **5** 28–44
[55] Gooding J J, Mearns F, Yang W and Liu J 2003 *Electroanalysis* **15** 81–96
[56] Liang J, Sun Q, Selloni A and Scoles G 2006 *J. Phys. Chem.* B **110** 24797–801
[57] Senaratne W, Andruzzi L and Ober C K 2005 *Biomacromolecules* **6** 2427–48
[58] Reed M A, Zhou C, Muller C J, Burgin T P and Tour J M 1997 *Science* **278** 252
[59] Sakotsubo Y, Ohgi T, Fujita D and Ootuka Y 2005 *Physica* E **29** 601
[60] Nuzzo R G, Dubois L H and Allara D L 1990 *J. Am. Chem. Soc.* **112** 558
[61] Poirier G E and Pylant E D 1996 *Science* **272** 1145
[62] Meshulam G, Rosenberg N, Caster A, Burstein L, Gozin M and Richter S 2005 *Small* **1** 848
[63] Bethell D, Brust M, Schiffrin D J and Kiely C 1996 *J. Electroanal. Chem.* **409** 137
[64] Harrell L E, Bigioni T P, Cullen W G, Whetten R L and First P N 1999 *J. Vac. Sci. Technol.* B **17** 2411
[65] Ohgi T, Sheng H-Y, Dong Z-C, Nejoh H and Fujita D 2001 *Appl. Phys. Lett.* **79** 2453
[66] Aslam M, Mulla I S and Vijayamohanan K 2001 *Langmuir* **17** 7487
[67] Bandyopadhyay K and Vijayamohanan K 1998 *Langmuir* **14** 6924
[68] Liu F-K, Hsu Y-T and Wu C-H 2005 *J. Chromatogr.* A **1083** 205
[69] Vandamme N, Snauwaert J, Janssens E, Vandeweert E, Lievens P and Van Haesendonck C 2004 *Surf. Sci.* **558** 57
[70] Noda H, Tai Y, Shaporenko A, Grunze M and Zharnikov M 2005 *J. Phys. Chem.* B **109** 22371
[71] Qu D and Uosaki K 2006 *J. Phys. Chem.* B **110** 17570
[72] Chen S 2000 *J. Phys. Chem.* B **104** 663
[73] de Boer B, Frank M M, Chabal Y J, Jiang W, Garfunkel E and Bao Z 2004 *Langmuir* **20** 1539

[74] Lioubashevski O, Chegel V I, Patolsky F, Katz E and Willner I 2004 *J. Am. Chem. Soc.* **126** 7133
[75] Xiao Y, Patolsky F, Katz E, Hainfeld J F and Willner I 2003 *Science* **299** 1877
[76] Erickson E S, Livanec P W, Frisz J F and Dunn R C 2009 *Langmuir* **25** 5098–102
[77] Pignataro B 2009 *J. Mater. Chem.* **19** 3338
[78] Zhang Y, Tong Y, Abe M, Uosaki K, Osawa M, Sasaki Y and Ye S 2009 *J. Mater. Chem.* **19** 261
[79] Mendes P M, Yeung C L and Preece J A 2007 *Nanoscale Res. Lett.* **2** 373
[80] Sader J E, Larson I, Mulvaney P and White L R 1995 *Rev. Sci. Instrum.* **66** 3789
[81] Sader J E 1995 *Rev. Sci. Instrum.* **66** 4583
[82] Sader J E, Chon J W M and Mulvaney P 1999 *Rev. Sci. Instrum.* **70** 3967
[83] San Paulo A and García R 2001 *Phys. Rev.* B **64** 193411
[84] García R and Pérez R 2002 *Surf. Sci. Rep.* **47** 197
[85] Lee M H and Jhe W H 2006 *Phys. Rev. Lett.* **97** 036104
[86] Kowalewski T and Legleiter J 2006 *J. Appl. Phys.* **99** 064903
[87] Kokavecz J, Horváth Z L and Mechler A 2004 *Appl. Phys. Lett.* **85** 3232
[88] Stark R W, Schitter G and Stemmer A 2003 *Phys. Rev.* B **68** 085401
[89] Baba A, Sato F, Fukuda N, Ushijima H and Yase K 2009 *Nanotechnology* **20** 085301
[90] Li B, Goh C F, Zhou X, Lu G, Tantang H, Chen Y, Xue C, Boey F Y C and Zhang H 2008 *Adv. Mater.* **20** 4873–8
[91] Martínez-Otero A, Hernando J, Ruiz-Molina D and Maspoch D 2008 *Small* **4** 2131–5
[92] Zheng Z, Jang J-W, Zheng G and Mirkin C A 2008 *Angew. Chem. Int. Edn* **47** 9951–4
[93] Zhang M, Bullen D, Chung S-W, Hong S, Ryu K S, Fan Z, Mirkin C A and Liu C 2002 *Nanotechnology* **13** 212–7
[94] Li Y, Maynor B W and Liu J 2001 *J. Am. Chem. Soc.* **123** 2105–6
[95] Seo K and Borguet E 2006 *Langmuir* **22** 1388–91
[96] Brower T L, Garno J C, Ulman A, Liu G-Y, Yan C, Gölzhäuser A and Grunze M 2002 *Langmuir* **18** 6207–16
[97] Hurley P T, Ribbe A E and Buriak J M 2003 *J. Am. Chem. Soc.* **125** 11334–9
[98] Vettiger P *et al* 2002 *IEEE Trans. Nanotechnol.* **1** 39–55
[99] Eleftheriou E *et al* 2003 *IEEE Trans. Magn.* **39** 938–45
[100] Dürig U *et al* 2000 *Tribol. Lett.* **9** 25–32
[101] Vettiger P, Despont M, Drechsler U, Dürig U, Häberle W, Lutwyche M I, Rothuizen H E, Stutz R, Widmer R and Binnig G K 2000 *IBM J. Res. Dev.* **44** 323–40
[102] Mateiu R, Kühle A, Marie R and Boisen A 2005 *Ultramicroscopy* **105** 233–7
[103] Leung T Y B, Gerstenberg M C, Lavrich D J, Scoles G, Schreiber F and Poirier G E 2000 *Langmuir* **16** 549
[104] Esplandiu M J, Carot M L, Cometto F P, Macagno V A and Patrito E M 2006 *Surf. Sci.* **600** 155
[105] Pontes R B, Novaes F D, Fazzio A and da Silva A J R 2006 *J. Am. Chem. Soc.* **128** 8996
[106] Bauschlicher C W and Ricca A 2003 *Chem. Phys. Lett.* **367** 90
[107] Jiang W, Zhitenev N, Bao Z, Meng H, Abusch-Magder D, Tennant D and Garfunkel E 2005 *Langmuir* **21** 8751
[108] Tai Y, Shaporenko A, Rong H T, Buck M, Eck W, Grunze M and Zharnikov M 2004 *J. Phys. Chem.* B **108** 16806
[109] Joo S W, Han S W and Kim K 2001 *J. Colloid Interface Sci.* **240** 391
[110] Tour J M, Jones L, Pearson D L, Lamba J J S, Burgin T P, Whitesides G M, Allara D L, Parikh A N and Atre S V 1995 *J. Am. Chem. Soc.* **117** 9529
[111] Kasibhatla B S T, Labonte A P, Zahid F, Reifenberger R G, Datta S and Kubiak C P 2003 *J. Phys. Chem.* B **107** 12378
[112] Niklewski A, Azzam W, Strunskus T, Fischer R A and Wöll C 2004 *Langmuir* **20** 8620
[113] Ulman A 1996 *Chem. Rev.* **96** 1533
[114] Love J C, Estroff L A, Kriebel J K, Nuzzo R G and Whitesides G M 2005 *Chem. Rev.* **105** 1103
[115] Wang W, Lee T and Reed M A 2005 *Rep. Prog. Phys.* **68** 523
[116] Brust M, Blass P M and Bard A J 1997 *Langmuir* **13** 5602
[117] Brower T L, Cook M and Ulman A 2003 *J. Phys. Chem.* B **107** 11721
[118] Liu G-Y, Xu S and Qian Y 2000 *Acc. Chem. Res.* **33** 457–66
[119] Kaholek M, Lee W-K, Ahn S-J, Ma H, Caster K C, LaMattina B and Zauscher S 2004 *Chem. Mater.* **16** 3688–96
[120] Chwang A B, Granstrom E L and Frisbie C D 2000 *Adv. Mater.* **12** 285–8
[121] Shi J, Chen J and Cremer P S 2008 *J. Am. Chem. Soc.* **130** 2718–9
[122] Kaholek M, Lee W-K, LaMattina B, Caster K C and Zauscher S 2004 *Nano Lett.* **4** 373–6
[123] Liang J, Rosa L G and Scoles G 2007 *J. Phys. Chem.* C **111** 17275–84
[124] Greene M E, Kinser C R, Kramer D E, Pingree L S C and Hersam M C 2004 *Microsc. Res. Tech.* **64** 415
[125] Garcia R, Martinez R V and Martinez J 2006 *J. Chem. Soc. Rev.* **35** 29
[126] Amro N A, Xu S and Liu G-Y 2000 *Langmuir* **16** 3006
[127] Jaschke M and Butt H-J 1995 *Langmuir* **11** 1061
[128] Senkevich J J, Mitchell C J, Yang G-R and Lu T-M 2002 *Langmuir* **18** 1587
[129] Sanderson R T 1976 *Chemical Bonds and Bond Energy* 2nd edn (New York: Academic) ISBN-10:0126180601
[130] Agarwal G, Sowards L A, Naik R R and Stone M O 2003 *J. Am. Chem. Soc.* **125** 580–3
[131] Liang J and Scoles G 2007 *Langmuir* **23** 6142–7
[132] Hansen L T, Kühle A, Sorensen A H, Bohr J and Lindelof P E 1998 *Nanotechnology* **9** 337
[133] García R, Calleja M and Rohrer H 1999 *J. Appl. Phys.* **86** 1898